PHYSICAL REVIEW D VOLUME 24, NUMBER 9 1 NOVEMBER 1981

Strange-particle production in neutrino scattering

H. K. Dewan
Department of Physics and Astrophysics, University of Delhi, Delhi-110007, India
(Received 1 December 1980)

Cross-section estimates are presented for strangeness-changing charged-current reactions $\nu_\mu N \to \mu Y \pi$, $\nu_\mu N \to \mu N K$, $\bar{\nu}_\mu N \to \mu^+ Y \pi$, and $\bar{\nu}_\mu N \to \mu^+ N K$. The reactions are considered within the Cabibbo theory with the current belonging to an octet of SU(3). The calculations are performed using Born approximations for a range of neutrino energies which cover both the Argonne and the Fermilab spectra. We find the flux-averaged cross section for $K^+ p$ final state to be in rough agreement with the value indicated by the Fermilab data.

I. INTRODUCTION

Recent experiments at Argonne[1] and at Fermilab[2] have indicated the production of hyperons and kaons in neutrino-nucleon scattering,[1,2] besides giving more detailed information on pion production. The pion-production processes have been studied in depth by various authors[3] and processes in which there is an associated production of strange particles have been studied by Shrock.[4] Shrock considers both charged- and neutral-current processes in the region of the ANL neutrino spectrum which is concentrated in the low-energy region. The processes considered by him can be written in general as $\nu N \to l K Y$ and $\nu N \to \nu K Y$, where Y refers to a Λ or a Σ hyperon. In this work, we extend Shrock's estimates of cross sections to the high-neutrino-energy region, where the Fermilab neutrino spectrum is concentrated, and also estimate the cross sections for $\Delta S = \pm 1$ production reactions in this scattering. These processes have no neutral-current contributions as they involve a change in strangeness and therefore in charge. One of these, $\nu p \to \mu^- K^+ p$, has been reported by both the ANL and Fermilab groups.[2]

The $\Delta S = \pm 1$ reactions are important because they afford a test of the Cabibbo theory and our understanding of strangeness-changing weak processes and therefore supplement the information obtained from the study of pion-production experiments.[5] The estimates for the processes considered here are smaller than the corresponding pion-production cross sections. The primary reason for this is our assumption that in the channels considered there are no low-lying resonances and the cross section is therefore not enhanced. [In contrast, for the pion-production processes in the $\Delta(1230)$ region nearly the whole of the cross section is resonant.[3]] Further, for the $|\Delta S| = 1$ processes, besides the fact that the cross section is damped by a factor of $\tan^2\theta_C$, the phase space available for most of these reactions is also smaller than that available in pion-production processes. The theoretical[1-3] and experimental estimates for the pion production show a rapid increase in cross section at low neutrino energies and then a leveling off to a near constant value at higher energies. Our theoretical estimates for processes involving strange particles in the final state follow almost the same pattern. The cross section rises with neutrino energy and levels off at higher neutrino energies. The major difference lies in the fact that it is at comparatively higher neutrino energies where the cross sections stop rising. At still higher energies the cross sections start falling slowly. The specific processes we have considered besides $\nu N \to \mu^- K^+ \Lambda$ are the $\Delta S = 1$ processes in which only one of the hadrons is strange, i.e., the final state is either a nucleon-kaon or a Y (Λ or Σ) -pion state. The initial state is a neutrino or antineutrino beam incident on nucleons. Although our estimates are made for an initial state, which has free nucleons, during actual experiments the nucleons are embedded in nuclei. Adler *et al.*[6] have calculated the corrections which have to be made to the theoretical estimates for comparison with experimental results. The corrections are, however, small and until detailed data is available on strange-particle production it would be premature to calculate these corrections.

The cross sections are calculated using the generalized Born graphs, but we have used the full form factors for the current-hadron vertices. This is a reasonable approximation near the threshold if there are no strong resonances near threshold in the production channel. For $K\Lambda, K\Sigma$ reactions this is well satisfied because in these the nearest resonances are $N^*(1700)$ and $N^*(1780)$, which decay mainly into πN and $\pi\pi N$ channels, and their decay into KY is less than 10%. The $K^+ p$ production channel is a barren channel with no resonances and therefore for this channel also our results are reasonably correct for low values of the hadronic center-of-mass energy W. In

principle, for high hadronic center-of-mass energies the calculation should be performed using Regge exchange, which would give a cross section falling with W for large W. Our results also have a similar pattern but obviously with a somewhat different slope. However, since in the integrated cross section the major contribution comes from the low-W region, our results for the integrated cross section are not expected to be very different from the results of a more complete calculation. In the event of more statistics being available we could compare our results by making a suitable cut in W at some low W, where our simple model is expected to have more validity. For the other channels $\bar{K}N$ or $Y\pi$, resonances do exist and therefore our estimates for the processes are perhaps not very good in the region of the resonances.[7]

Strange particles have been reportedly observed by the ANL[1] and Fermilab[2] groups. The ANL observations are with a spectrum which is peaked around low neutrino energies (the peak is at 0.5 GeV with 90% of the spectrum below 1.5 GeV and 96% below 2 GeV). On the other hand, the Fermilab neutrino spectrum is concentrated at high energies. The spectrum is constant between 10–30 GeV and then falls off such that 90% of the flux lies below 100 GeV. It is important for us to know the flux spectrum if we want to compare theory with experiment. Our calculations give us a cross section dependent on W and E_ν, which we label as $\sigma(W, E_\nu)$. The experimentalist, however, measures the cross section due to the whole neutrino spectrum which is a weighted average of $\sigma(W, E_\nu)$ with the weight of each E_ν being given by the flux shape at that point. Thus

$$\frac{d\bar{\sigma}}{dW} = \int \sigma(W, E_\nu) f(E_\nu) dE_\nu \Big/ \int f(E_\nu) dE_\nu , \qquad (1)$$

where $f(E_\nu)$ is the incident-neutrino-flux shape. The scanty data available for the channels considered does not allow a meaningful comparison between theory and experiment for $d\bar{\sigma}/dW$. The data available is in terms of a total number of events in that channel which implies that we calculate $\bar{\sigma} = \int (d\bar{\sigma}/dW) dW$ and compare $\bar{\sigma}$ with the experimental numbers. It is clear from the nature of the neutrino spectrum itself that the ANL cross section would be low, because for those neutrino energies at which the flux peaks the cross section is negligible. For the higher-energy spectrum, however, the cross section would be appreciably larger, and could, with more statistics, become available as a function of W.

II. CALCULATIONS

The strangeness-changing processes under consideration can be written concisely in the form

$$\nu(\bar{\nu})(k_1) + N(p_1) \to l(l^*)(k_2) + Y(p_2) + \pi(q) \qquad (2)$$

and

$$\nu(\bar{\nu})(k_1) + N(p_1) \to l(l^*)(k_2) + N(p_2) + \bar{K}(q) . \qquad (3)$$

Here Y refers to a strange baryon Λ or Σ; N to a nucleon, and the quantities in parenthesis are the momentum labels of the particles. For the associated production reactions we only consider $\nu(k_1) + n(p_1) \to \mu^- K^+ \Lambda$. As we have already said, this is being considered because we want to extend Shrock's calculations to the region of the Fermilab spectrum. The general nature of the Born graphs for the $\Delta S = \pm 1$ processes considered is shown in Fig. 1.

The initial state is a neutrino or an antineutrino incident on a nucleon target. As mentioned earlier, we have not considered the corrections to the cross sections arising, due to the fact that the interacting nucleons in experiments are not free particles but are a part of a nucleus. This correction, however, is not important at the moment because the available data is too low for a meaningful comparison in detail and also because our estimates anyway are not precise enough to be sensitive to these corrections. These processes in general include either a Σ pole or both Σ and Λ poles in the s channel, a K (K^*) or a π pole in the t channel, and a nucleon or a Σ or Σ and Λ poles in the u channel. In our estimates, we do not include the contributions of N^* and Y^* resonances in the s or u channels and higher meson resonances in the t channel, and restrict ourselves to forces generated by a baryon octet and a pseudoscalar-meson octet. This is in the spirit of single-pion-production calcula-

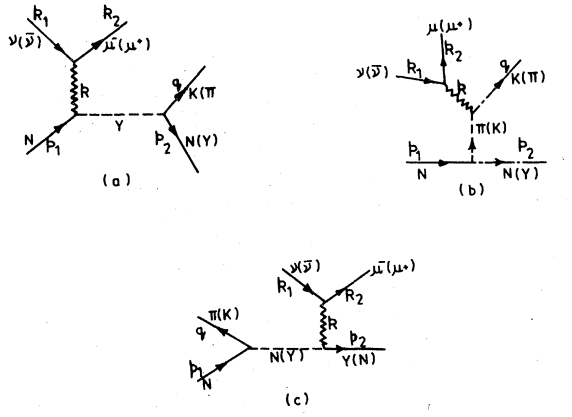

FIG. 1. General nature of Born diagrams contributing to the cross section. (a) s-channel baryon exchange, (b) t-channel meson exchange, (c) u-channel baryon exchange. k is the momentum transfer carried by the current.

tions of Refs. 3(a) and 3(b) and kaon-production calculations of Ref. 4. We do not consider the effect of K^* exchange, primarily because we do not have any information on the axial-vector coupling strength of the K^*-K-current vertex. The vector coupling (KK^*J_μ) can, in principle, be obtained from photoproduction data and from that using SU(3) symmetry some estimate for the ($\pi K^* J_\mu$) vertex can be obtained. Shrock,[4] however, has estimated the difference due to the inclusion of the K^*-exchange vector amplitude in the K-Λ reactions to be 5–20%, depending on the reaction. We expect that for $\Delta S \neq 0$ processes the corrections would be of the same order, and hence do not consider K^* exchange in these calculations.

The invariant matrix element for these processes is

$$\mathfrak{M} = \left(\frac{G}{\sqrt{2}}\right) l_\mu \langle q p_2 | J^\mu | p_1 \rangle , \tag{4}$$

where

$$l_\mu = \bar{U}_{l,l^*}(k_2)\gamma_\mu(1 \mp \gamma_5) U_{\nu(\bar{\nu})}(k_1) . \tag{5}$$

The standard $\Delta S = 1$ $V-A$ Cabibbo current is given as

$$J^\mu = \sin\theta_C (F^\mu_{4+i5} - F^{5\mu}_{4+i5}) , \tag{6}$$

where $\sin\theta_C \sim 0.243$. To determine the interaction at the current vertex of the Born diagrams we use the SU(3) relations

$$\langle i | F^\mu_j | k \rangle = d_{ijk} D^\mu_V + i f_{ijk} F^\mu_V , \tag{7}$$

$$\langle i | F^{5\mu}_j | k \rangle = d_{ijk} D^\mu_A + i f_{ijk} F^\mu_A . \tag{8}$$

Here i, j, and k are SU(3) labels of the octet and f_{ijk} and d_{ijk} are the antisymmetric and the symmetric structure constants of SU(3). In this we have assumed that the vector and the axial-vector currents each form an octet of their own. D^μ_V and F^μ_V can be expressed in terms of nucleon form factors

$$D^\mu_V = -\tfrac{3}{2} \langle n | J^\mu_{\rm em} | n \rangle , \tag{9}$$

$$F^\mu_V = \langle p | J^\mu_{\rm em} | p \rangle + \tfrac{1}{2} \langle n | J^\mu_{\rm em} | n \rangle . \tag{10}$$

The forms of $\langle n | J^\mu_{\rm em} | n \rangle$ and $\langle p | J^\mu_{\rm em} | p \rangle$ are of course well known. Similarly, for the axial-vector current

$$D^\mu_A = \left(\frac{D}{D+F}\right) \langle p | F^{5\mu}_{1+i2} | n \rangle , \tag{11}$$

$$F^\mu_A = \left(\frac{F}{D+F}\right) \langle p | F^{5\mu}_{1+i2} | n \rangle , \tag{12}$$

where

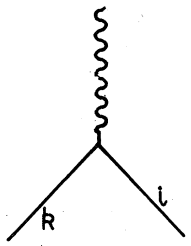

FIG. 2. A general s- or u-channel current vertex; j is the current index and k and i are the final and initial baryons at the current vertex.

$$\langle p | F^{5\mu}_{1+i2} | n \rangle = (D+F) F_A(k^2) \bar{U}_p \gamma_\mu \gamma_5 U_n \tag{13}$$

with

$$F_A(k^2) = \frac{1}{(1 - k^2/m_A^{\,2})^2} , \tag{14}$$

$m_A \simeq 0.95$, $D = 0.78 \pm 0.02$, and $F = 0.45 \pm 0.02$.[4]

The forms we use for the s,u-channel current vertices are

$$i\gamma_\lambda F^{ijk}_1(k^2) - i\sigma_{\lambda\eta} k_\eta F^{ijk}_2(k^2) + i\gamma_\lambda\gamma_5 g_A(k^2) + \gamma_5 k_\lambda h_A(k^2) , \tag{15}$$

where F^{ijk}_1, F^{ijk}_2 represent the vector form factors for the current vertex and g^{ijk}_A, h^{ijk}_A represent the axial-vector form factors (see Fig. 2). We include the induced isoscalar term $\gamma_5 k_\lambda h_A$, even though it is proportional to the lepton mass term on contraction with the lepton current. For the t channel, except for the associated-production case, the vertices are of the form shown in Fig. 3 with a contribution $\langle K(\pi) | J^\mu | \pi(K) \rangle$. These form factors can be deduced from kaon decay experiments and have been taken from Ref. 8. We assume the absence of second-class currents so that no terms of the form q_μ or $i\sigma_{\mu\nu} q_\nu \gamma_5$ appear in the matrix element. We also assume that the divergence of the vector current is zero which implies that it is a conserved current. We also assume extended PCAC (partial conservation of

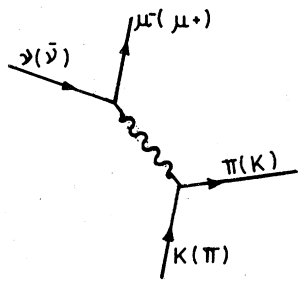

FIG. 3. t-channel diagram for $\Delta S = \pm 1$ scattering process.

axial-vector current) for the divergence of the axial-vector current. For these processes the Goldberger-Treiman relation is beset with the difficulty that the pole at m_K^2 is not far removed from the continuum starting at $(m_K+m_\pi)^2$. It is for this reason that the approximation of the K pole dominating for $|\Delta S|=1$ processes is not very good.

For calculations we follow the technique used by Adler in his classic paper on weak production of pions.[3(b)] We choose the invariants

$$\begin{aligned}
O(V_1)&=\tfrac{1}{2}i\gamma_5(\gamma\cdot l\gamma\cdot k-\gamma\cdot k\gamma\cdot l)\,,\\
O(V_2)&=2i\gamma_5(P\cdot lq\cdot k-q\cdot lP\cdot k)\,,\\
O(V_3)&=\gamma_5(\gamma\cdot lq\cdot k-\gamma\cdot kq\cdot l)\,,\\
O(V_4)&=2\gamma_5[(\gamma\cdot lP\cdot k-\gamma\cdot kP\cdot l)\\
&\quad-\frac{iM_n}{2}(\gamma\cdot l\gamma\cdot k-\gamma\cdot k\gamma\cdot l)]\,,\\
O(V_5)&=i\gamma_5(k\cdot lq\cdot k-k^2q\cdot l)\,,\\
O(V_6)&=\gamma_5(k\cdot l\gamma\cdot k-k^2\gamma\cdot l)
\end{aligned}\tag{16}$$

for vector current. Here $P=\frac{1}{2}(p_1+p_2)$ and $q=(p_1+k-p_2)$; similarly

$$\begin{aligned}
O(A_1)&=\tfrac{1}{2}i(\gamma\cdot q\gamma\cdot l-\gamma\cdot l\gamma\cdot q)\,,\\
O(A_2)&=2iP\cdot l\,,\\
O(A_3)&=iq\cdot l\,,\\
O(A_4)&=-M_n\gamma\cdot l\,,\\
O(A_5)&=-2\gamma\cdot kP\cdot l\,,\\
O(A_6)&=-\gamma\cdot kq\cdot l\,,\\
O(A_7)&=ik\cdot l\,,\\
O(A_8)&=-\gamma\cdot kk\cdot l\,,
\end{aligned}\tag{17}$$

are the invariants for the axial-vector current.

There are only six linearly independent amplitudes for the vector current because of the conservation of vector current $\partial_\mu J_\mu^V=0$ and each Born graph can be expressed in terms of the above invariants. If M_λ is the hadronic contribution of the diagram, then

$$l_\lambda M_\lambda^V=\sum_{i=1}^{6}V_i(\nu,\nu_B,k^2)\bar{U}(p_2)O(V_i)U(p_1)\tag{18}$$

and

$$l_\lambda M_\lambda^A=\sum_{i=1}^{8}A_i(\nu,\nu_B,k^2)\bar{U}(p_2)O(A_i)U(p_1)\,,\tag{19}$$

where $\nu=-P\cdot k/M$ and $\nu_B=q\cdot k/2M$. The amplitudes are

$$\begin{aligned}
V_1&=\frac{-G_s}{(W^2-M_s^{\,2})}[F_{1s}^V+(M_s-M_n)F_{2s}^V]\\
&\quad+\frac{G_u}{(q^2-2p_1\cdot q)}[F_{1u}^V+(M_F-M_u)F_{2u}^V]\,.
\end{aligned}$$

Here G_s, and G_u refer to the renormalized coupling constants at the strong vertices of the s and u channels, respectively, M_N is the initial nucleon mass, M_F is the mass of the final baryon, and M_s and M_u are the masses of the intermediate particles exchanged in the s and u channels, respectively. Similar labels would be used for the t channel also. F_{1s}^V, F_{2s}^V, etc. are the form factors at the current vertices of the s and u channel (calculated as explained above), equivalent to the p-n electromagnetic form factors. For each additional diagram in the s or u channel a similar term would be added to V_1 with a negative sign for additional diagrams in the s channel and positive sign for diagrams in the u channel. We define

$$\frac{G_s}{(W^2-M_s^{\,2})}=G_{s1};\quad(M_s-M_n)=\Delta M_s$$

and

$$\frac{G_u}{(q^2-2p_1\cdot q)}=G_{u1};\quad(M_F-M_u)=\Delta M_u\,.$$

Then

$$V_1=G_{s1}(F_{1s}^V+\Delta M_sF_{2s}^V)+G_{u1}(F_{1u}^V+\Delta M_uF_{2u}^V),\tag{20}$$

$$V_2=\frac{G_{s1}F_{1s}^V}{q\cdot k}-\frac{G_{u1}F_{1u}^V}{q\cdot k}\,,\tag{21}$$

$$V_3=G_{s1}F_{2s}^V+G_{u1}F_{2u}^V\,,\tag{22}$$

$$V_4=G_{s1}F_{2s}^V-G_{u1}F_{2u}^V\,,\tag{23}$$

$$\begin{aligned}
k^2V_5&=G_{s1}(W^2-M_n^{\,2})\frac{F_{1s}^V}{q\cdot k}+\frac{G_TF_K}{(k^2+2q\cdot k+q^2-m_T^{\,2})}\\
&\quad-G_{u1}\frac{F_{1u}^V}{q\cdot k}(W^2-M_n^{\,2}+2q\cdot k);
\end{aligned}\tag{24}$$

here G_T is the t-channel strong coupling constant, F_K is the current-pion-kaon vertex weak form factor, and M_T is the mass of the exchanged particle in the t channel; also

$$V_6=G_{s1}\Delta M_sF_{1s}^V-G_{u1}F_{1u}^V\Delta M_u\,.\tag{25}$$

In the limit of exact SU(3) symmetry all the mass differences are zero and therefore V_6 is also zero.

Similarly for the axial-vector current amplitudes we have

$$A_1=G_{s1}G_A^s-G_{u1}G_A^u\,,\tag{26}$$

where G_A^s and G_A^u are the s- and u-channel axial-vector form factor equivalent to $g_A(k^2)$ for the current-p-n vertex. We use similar notation for the induced pseudoscalar form factors. We obtain

$$A_3 = G_{s1} G_A^s - G_{u1} G_A^u , \tag{27}$$

$$A_4 = \frac{G_{s1} G_A^s}{M_n} (M_F - M_s) - \frac{G_{u1} G_A^u}{M_n} (M_u - M_n) , \tag{28}$$

$$A_7 = G_{s1} H_A^s \Delta M_s + G_{u1} H_A^u \Delta M_u , \tag{29}$$

$$A_8 = G_{s1} H_A^s + G_{u1} H_A^u , \tag{30}$$

$$A_2 = A_5 = A_6 = 0 . \tag{31}$$

We define

$$V_{34} = V_3 - V_4 \tag{32}$$

and

$$V_{25} = (W^2 - M_n^2) V_2 - k^2 V_5 . \tag{33}$$

To simplify calculations we will work in the isobaric frame of reference defined as $\vec{p}_2 + \vec{q} = 0$ (see Fig. 4) and express these invariant amplitudes in terms of the isobaric-frame amplitudes

$$e_\lambda M_\lambda^V = \sum_{j=1}^{6} \mathfrak{F}_j^V \chi_f^* \Sigma_j^V \chi_i \tag{34}$$

and

$$e_\lambda M_\lambda^A = \sum_{j=1}^{8} \mathfrak{g}_j^A \chi_f^* \Lambda_j^A \chi_i , \tag{35}$$

where χ_i and χ_f are the Pauli spinors of initial and final baryons and Σ_j^V and Λ_j^A are as used by Adler.[3(b)] The transformations connecting V_j's with F_j^V's and A_j''s with $\mathfrak{g}_j^A$'s are the same as in the appendix of Ref. 3, if SU(3) symmetry is exact and both initial and final baryons have the same mass. If initial and final baryons do not have the same mass, the normalization factor of the final spinor becomes $[(p_{20} + M_F)/2M_F]^{1/2}$ in place of $[(p_{20} + M_n)/2M_n]^{1/2}$. The other terms of the transformations remain unaltered.

These isobaric-frame amplitudes can be expressed in terms of helicity amplitudes as defined in Ref. 3(b) and the cross section can then be conveniently expressed in terms of these helicity amplitudes. Each of the helicity amplitudes is labeled by the initial-nucleon helicity, the lepton-pair helicity, and the final-nucleon helicity, as there is no other independent helicity available, the pion helicity being zero anyway. For the vector case, out of the 12 different helicity combinations possible, only six are effectively independent. The other six are related by phase factors to these by crossing symmetry. The six independent ones are chosen to be those which carry a different initial-nucleon helicity label or a different lepton-pair helicity label. For the axial case, besided the above six there are two more, as the axial-vector current has a nonzero divergence. Helicity amplitudes with different helicity labels do not mix and all such interference terms are zero. The matrix element squared is the sum squared of six $V-A$ helicity amplitudes and the two scalar amplitudes which have a contribution only from the axial-vector current. These two would vanish if the axial-vector current was conserved and are proportional to the lepton mass term. We retain in them only the residues of those forms which have an explicit pion pole. The contribution of the other terms would be very small.

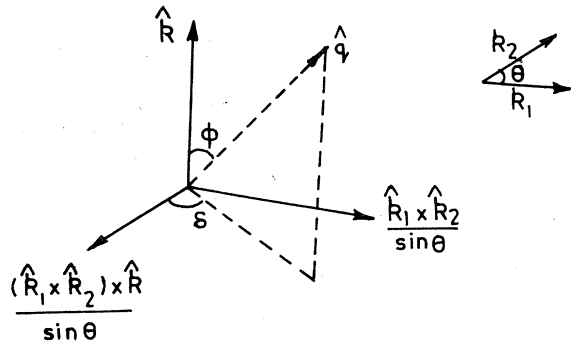

FIG. 4. Axes and angles specifying the final-lepton and the final-pion direction in the isobaric frame. $\hat{k}$ is the direction of lepton momentum transfer. θ is the lepton scattering angle, ϕ is the angle between pion-emission direction and $\hat{k}$, and δ is the angle the emerging pion makes with the lepton scattering plane.

The fully differential cross section is

$$\frac{d^3\sigma}{dk^2 dW d\Omega_\pi} = \frac{G^2 |\vec{q}|}{16 M_n^2 E_\nu^2 (2\pi)^5 W} L_{\mu\nu} W^{\mu\nu} . \tag{36}$$

$L_{\mu\nu}$ is the leptonic and $W^{\mu\nu}$ the hadronic part,

$$L_{\mu\nu} = (k_{1\mu} k_{2\nu} + k_{2\mu} k_{1\nu} - k_1 \cdot k_2 g_{\mu\nu} - i\xi \epsilon_{\mu\nu\alpha\beta} k_1^\alpha k_2^\beta) , \tag{37}$$

where $\xi = +1$ for initial neutrinos and $\xi = -1$ for antineutrinos

$$W^{\mu\nu} = \tfrac{1}{2} \sum_{\text{spins}} \langle KY|J^\mu|N\rangle \langle KY|J^\nu|N\rangle^* . \tag{38}$$

The product $L_{\mu\nu} W^{\mu\nu}$ is expressible in terms of helicity amplitudes; therefore in the decomposition

$$L_{\mu\nu} W^{\mu\nu} = T_0 + T_1 \cos\delta + T_2 \cos 2\delta + T_3 \sin\delta + T_4 \sin 2\delta \tag{39}$$

the T's are in terms of helicity amplitudes. If we are interested in total production we need to integrate over k^2, W, and Ω_π. The $d\Omega_\pi$ integral

is an integral over the pion angles ϕ and δ. Out of these the δ integral is trivial and gives simply $2\pi T_0$. The k^2 and ϕ integrations were done numerically on a computer. The δ integral extends simply from 0 to π while the k^2 integral extends in the limit of negligible muon mass from 0 to

$$\frac{2M_n k_{10}^L (2M_n k_{10}^L + M_N{}^2 - W^2)}{(M_n{}^2 + 2M_n k_{10}^L)} .$$

The only quantities not yet specified are the strong coupling constants. For these, we use experimental results[9] coupled with the SU(3) predictions.[8] This is a serious source of uncertainty in our analysis because the constants are not exactly known and are only specified to a range. For coupling constants for which no experimental numbers are available, the SU(3) values have to be used even though we know that these may not be very good. The coupling constants we need are $g_{NN\pi}$, $g_{NK\Sigma}$, $g_{\Sigma\Sigma\pi}$, $g_{NK\Lambda}$, and $g_{\Lambda\pi\Sigma}$. Out of these $g_{NN\pi}$ is well known and is given by $g_{NN\pi}{}^2/4\pi \sim 14.6$. For the others we give the SU(3) values as well as the experimental values in Table I (where $\alpha = D/D+F$). The $\Sigma\Sigma\pi$ coupling is of the type $\bar{\Sigma}\times\Sigma\cdot\pi$, which implies among other things that $g_{\Sigma^0\Sigma^0\pi^0}=0$ and all $\Sigma\Sigma\pi$ constants do not have the same sign; for example,

$$g_{\bar{\Sigma}^-\Sigma^-\pi^0} = -g_{\bar{\Sigma}^+\Sigma^+\pi^0} .$$

Each process considered has its own distinctive features depending on the channels open, the current hadron vertex form factors, and the coupling constant of the strong vertex. The characteristic features are the following:

(1) $\nu p \to \mu^- K^+ p$. No s-channel diagram and two u-channel diagrams but because of the fact that $g_{NK\Sigma}/g_{NK\Lambda} \ll 1$, the second diagram has a very small contribution.

(2) $\bar{\nu} p \to \mu^+ K^- p$. No u channel allowed, but two diagrams in the s channel with one dominating as in the u channel of the above process for the same reason.

(3) $\nu n \to \mu^- K^0 p$. No s-channel diagram and two u-channel diagrams with the Λ-pole diagram dominating.

(4) $\bar{\nu} n \to \mu^+ K^- n$. No u-channel diagram exists.

(5) $\nu n \to \mu^- K^+ n$. No s-channel diagram allowed and because $g_{NK\Sigma}/g_{NN\pi} \ll 1$ it is really the t channel which dominates.

(6) $\bar{\nu} n \to \mu^+ \Lambda \pi^-$. All diagrams allowed.

(7) $\bar{\nu} p \to \mu^+ \Lambda \pi^0$. All channels open; the s channel has two diagrams.

(8) $\bar{\nu} p \to \mu^+ \Sigma^0 \pi^0$. All diagrams allowed but the t channel diagram is very small.

(9) $\bar{\nu} p \to \mu^+ \Sigma^- \pi^+$. No t-channel diagram allowed.

(10) $\bar{\nu} p \to \mu^+ \Sigma^+ \pi^-$. No u-channel diagram allowed and the t channel is very small.

(11) $\bar{\nu} n \to \mu^+ \Sigma^- \pi^0$. The t channel has a very small contribution.

(12) $\bar{\nu} n \to \mu^+ \Sigma^0 \pi^-$. The t-channel diagram has only a small contribution.

(13) $\nu p \to \mu^- \pi^+ \Sigma^+$, $\nu n \to \mu^- \pi^+ \Lambda(\Sigma^0)$, and $\nu n \to \mu^- \pi^0 \Sigma^+$. In all these processes the s and the u channels are not allowed and at best the t channel is allowed with a small coupling constant only. We expect these cross section to be many times lower than the other processes considered here.

In all these $\Delta S \neq 0$ processes the $\Delta S = +1$ processes involve the neutrino, whereas the $\Delta S = -1$ processes involve antineutrinos.

III. RESULTS

The behavior of the cross sections as a function of W and E_ν calculated using the Born graphs is similar for all the processes that we have considered. We show the nature of the behavior by presenting the results for $\nu p \to \mu^- K^+ p$ in detail. For each of the other processes we present the $d\sigma/dW$ versus W plot for one representative value of the neutrino (antineutrino) energy (Figs. 5 and 6) and the flux-averaged total cross section using the Fermilab flux. We have chosen to present $\nu p \to \mu^- K^+ p$ in detail because it is the only $\Delta S \neq 0$

TABLE I. The experimental SU(3) values of the strong coupling constants along with the values of these constants used in this calculation.

Coupling constant	SU(3) values	Experimental range		Values used
$g_{\Sigma KN}$	$-g(1-2\alpha) \sim 3.6$	1.3	2.5	1.3 and wherever relevant 2.5
$g_{\Lambda KN}$	$-\frac{g(3-2\alpha)}{\sqrt{3}} \sim -13.5$	−10	−14	−10 and −13.5
$g_{\Lambda\pi\Sigma}$	$\frac{2\alpha g}{\sqrt{3}} \sim 10$	10.5	12.9	11
$\lvert g_{\Sigma\Sigma\pi}\rvert$	$2g(1-\alpha) \sim 10$	4	14	5 and 12

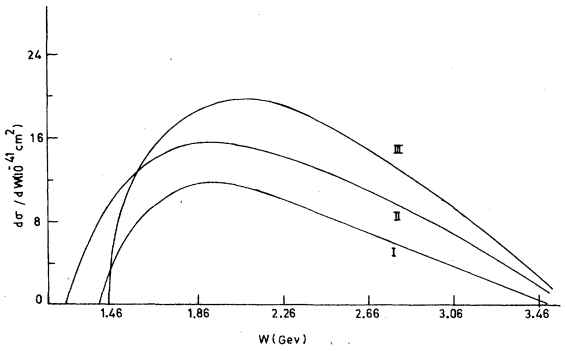

FIG. 5. $d\sigma/dW$ versus W curves for the processes (I) $\nu n \to \mu^- K^+ n$, (II) $\bar{\nu} p \to \mu^+ \Lambda \pi^0$, and (III) $\nu n \to \mu^- K^0 p$, respectively. Ths incident neutrino energy is 7 GeV.

channel which does not have any resonances and for which an experimental cross section is available for comparison. The results for $\nu p \to \mu^- K^+ p$ are shown in Figs. 7–11. In Fig. 7 $d\sigma/dW$ is plotted as a function of W, the mass of the hadronic pair, for various values of incident neutrino energies both in the region of Fermilab as well as Argonne spectra. In Fig. 8 we show the total cross section as a function of incident neutrino energy. In Fig. 9 we show $d\sigma/dW$ as a function of k_{10}^L, the incident neutrino energy, for various values of W. In Fig. 10 we present $d\sigma/dW$ calculated using two different values (−10 and −13.5) of the uncertain strong coupling constant $g_{NK\Lambda}$. In Fig. 12 we present results for a antineutrino scattering process $\bar{\nu} n \to \mu^+ \Lambda \pi^-$, which has contributions from all three channels and in Fig. 13 we present results for the associated production reaction $\nu n \to \mu^- K^+ \Lambda$ which receives almost no contribution from the u channel.

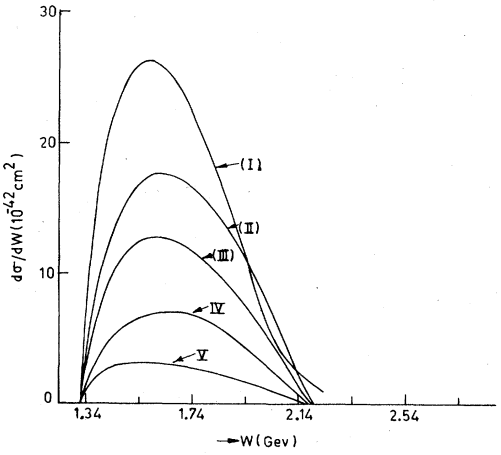

FIG. 6. $d\sigma/dW$ versus W curves for the following processes: (I) $\bar{\nu} p \to \mu^+ \Sigma^+ \pi^-$, (II) $\bar{\nu} p \to \mu^+ \Sigma^- \pi^+$ with the strong coupling constant $g_{\Sigma\Sigma\pi} = -12.0$, (III) $\bar{\nu} p \to \mu^+ \Sigma^- \pi^+$, $g_{\Sigma\Sigma\pi} = -5.0$, (IV) $\bar{\nu} p \to \mu^+ \Sigma^0 \pi^0$, and (V) $\bar{\nu} n \to \mu^+ \Sigma^0 \pi^-$. All these curves are plotted for an incident neutrino energy = 3 GeV.

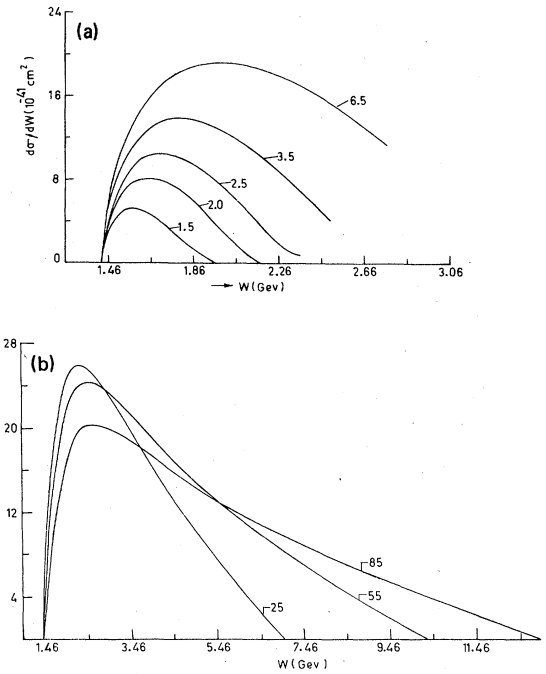

FIG. 7. $d\sigma/dW$ for $\nu p \to \mu^- K^+ p$ plotted against W for different neutrino energies; (a) at low neutrino energies and (b) at high neutrino energies. The neutrino energy in GeV for each curve is indicated with the curve.

It can be seen from Fig. 7 that $d\sigma/dW$ rapidly increases from zero as the hadronic mass increases beyond threshold. The cross section eventually reaches a maximum value, levels off, and then starts falling if the hadronic mass is in-

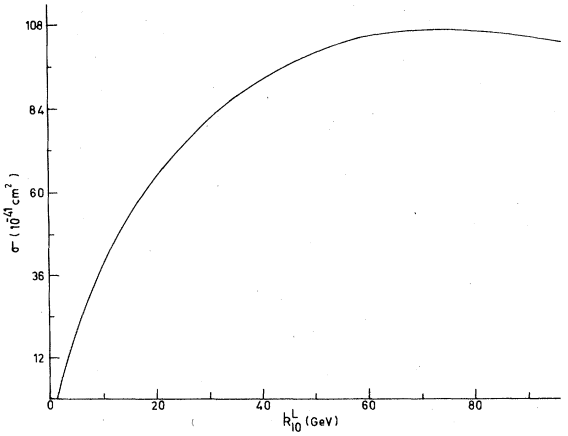

FIG. 8. σ plotted as a function of incident neutrino energy k_{10}^L for $\nu p \to \mu^- K^+ p$.

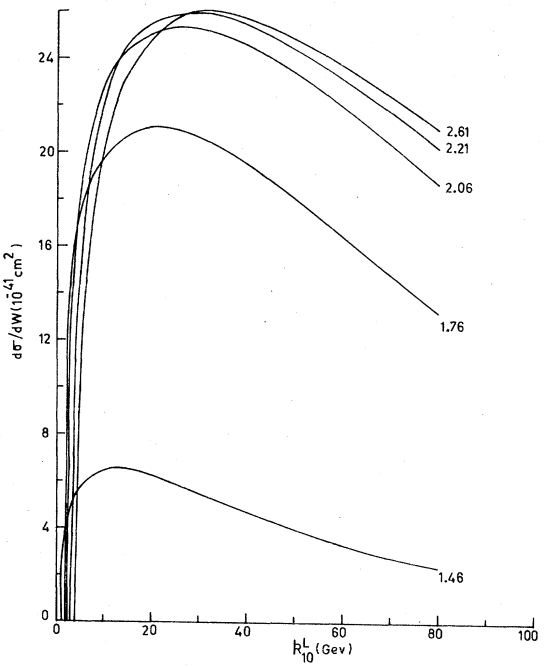

FIG. 9. $d\sigma/dW$ plotted against k^L_{10} at different values of the hadronic mass W. The hadronic mass in GeV for each particular curve is indicated with the curve.

creased any further. This feature is common to all the curves. The rate of fall of $d\sigma/dW$ for hadronic masses larger than the value at which $d\sigma/dW$ has a peak; the magnitude and the location of the peak, however, are different for different incident neutrino energies. The cross section at low neutrino energies falls fairly steeply and goes to zero rapidly. As the incident neutrino energy increases the tailing off keeps becoming slower such that at very high neutrino energies the cross section for fairly large hadronic masses is sizeable. The reasons for this is that at low neutrino energies it is not kinematically (energetically) possible to produce a very-high-mass hadronic system and the phase space allowed for the larger W values is considerably smaller. For high incident neutrino energies, however, there is no kinematic difficulty in producing a high-mass hadronic system and the phase space available does not change appreciably even for a considerable change in value of W. The cross section, in the high-neutrino-energy region [Fig. 7(b)] in contrast to the phase-space-limited low-incident-energy region [Fig. 7(a)] is primarily dependent on dynamics. The cross section $d\sigma/dW$

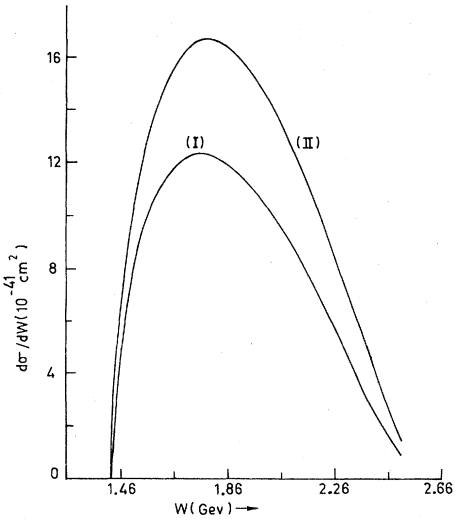

FIG. 10. $d\sigma/dW$ for $\nu p \to \mu^- K^+ p$ plotted as a function of W for two different values of the $NK\Lambda$ coupling. Curves labeled (I) and (II) correspond, respectively, to (I) $g_{NK\Lambda} \sim -10$ and (II) $g_{NK\Lambda} \sim -13.5$.

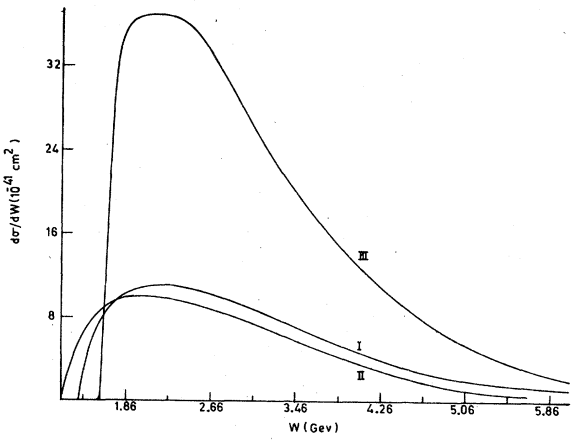

FIG. 11. Flux-averaged cross section ($d\bar{\sigma}/dW$) averaged over the Fermilab flux is plotted against W. The processes considered are, respectively, curve (I) $\nu p \to \mu^- K^+ p$, (II) $\bar{\nu} n \to \mu^+ \Lambda \pi^-$, and (III) $\nu n \to \mu^- K^+ \Lambda$.

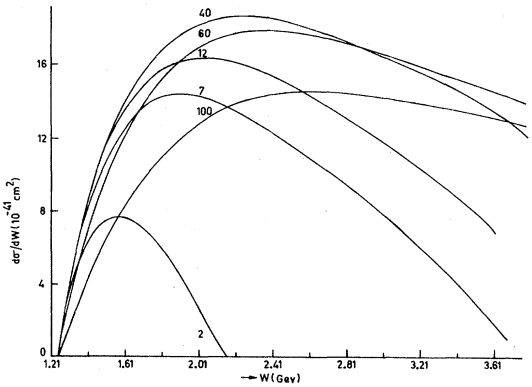

FIG. 12. $d\sigma/dW$ for $\bar{\nu} n \to \mu^+ \Lambda \pi^-$ plotted against W for different neutrino energies. The neutrino energy for each curve in GeV is indicated with that curve.

for all incident neutrino energies as W is increased eventually becomes zero whenever the kinematic cutoff for that neutrino energy is reached. The peak of the $d\sigma/dW$ curve keeps shifting towards higher hadronic masses as the neutrino energy increases. For example the K^+p threshold is 1.43 GeV and the peak of the $d\sigma/dW$ curve for k^L_{10} = 2 GeV occurs at 1.66 GeV, while for k^L_{10} = 40 GeV the peak occurs at 2.36 GeV. The peak value of $d\sigma/dW$ increases with k^L_{10} up to a certain maximum value and then starts falling. This can be seen in Fig. 7(b), where the higher-k^L_{10} curves have moved inside the lower-k^L_{10} curves. The fall is slow and occurs because the increase with k^L_{10} in the other factors of $d\sigma/dW$ is less than the damping factor $(k^L_{10})^2$ in the denominator. To understand this we note that initially as k^L_{10} increases from zero the available phase space increases, i.e., higher k^2 values are allowed and $d\sigma/dW$ increases. The increase in $d\sigma/dW$, however, keeps becoming slower as k^2 increases due to the $(k^2)^{-2}$-dependent form factors. The cross section $d\sigma/dW$ starts falling the moment the increase in the integral due to the additional available k^2 fails to offset the damping term. The higher-neutrino-energy curves therefore lie below the lower-neutrino-energy curves but they entend to higher hadronic masses because it becomes energetically possible, as k^L_{10} increases, for these high hadronic masses to be produced. The fact that the $d\sigma/dW$ vs W plots for higher neutrino energies are flatter and have a slower rate of fall implies that the total cross section $\sigma(k^L_{10})$ (area under the $d\sigma/dW$ curve) will nearly become independent of k^L_{10} for large k^L_{10} (Fig. 8).

We have calculated the flux-averaged cross section for all the processes using the Fermilab neutrino (antineutrino) spectra. (We have used the broadband-horn spectrum for neutrinos and the quadupole spectrum for antineutrinos.) The flux-averaged cross section

$$\bar{\sigma} = \frac{\int \sigma(k^L_{10})\,\phi(k^L_{10})\,dk^L_{10}}{\int \phi(k^L_{10})\,dk^L_{10}}$$

[k^L_{10} is the incident ν ($\bar{\nu}$) energy and $\phi(k^L_{10})$ is the flux shape.] We present for comparison the flux-averaged cross section for $\nu p \to \mu^- K^+ p$ and $\nu n \to \mu^- K^+ \Lambda$ using the ANL neutrino flux and for $\bar{\nu} n \to \mu^+ \Lambda \pi^-$ using the ANL antineutrino flux. The cross sections in this region are extremely small and are severely conditioned by phase-space restrictions. This is evident from the fact that the cross section for the lowest-mass hadronic system is the maximum and both the $\Delta S \neq 0$ processes, inspite of being damped by $\tan^2\theta_C$, have a cross section larger than the cross section for the $\Delta S = 0$ process $\nu n \to \mu^- K^+ \Lambda$. The results are presented in Table II. The Fermilab group[2] has measured the cross section for the first process to be $(14 \pm 8) \times 10^{-41}$ cm^2; this agrees with our theoretical number. There is no data available for any of the other processes at the Fermilab energies; however, at Argonne[1] other processes have also been reported. For $\nu n \to \mu^- K^+ \Lambda$ using the ANL data the cross section has been worked out to be $\sim 2 \times 10^{-41}$ cm^2 and for $\nu p \to \mu^- K^+ p$ the cross section $\sim 10^{-41}$ cm^2. Both the experimental numbers are of the same order but higher than our theoretical estimates. They are, however, estimated from very-low-statistics data so that the cross section is not very reliable. The re-

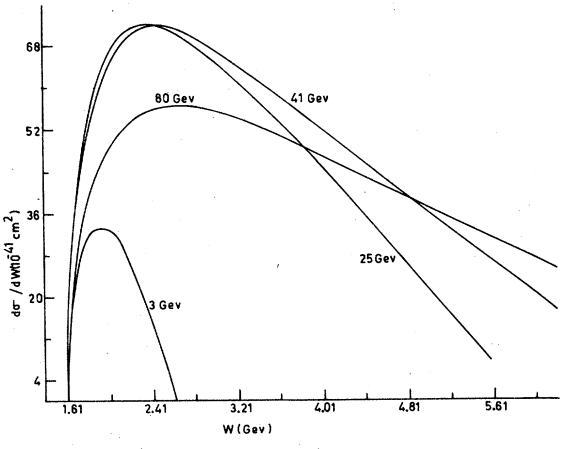

FIG. 13. $d\sigma/dW$ for $\nu n \to \mu^- K^+ \Lambda$ plotted against W for different neutrino energies. The neutrino energy in GeV for each curve is indicated with that curve.

TABLE II. Flux-averaged cross sections for the processes considered. For $\bar{\nu} p \to \mu^+ \Sigma^- \pi^+$, (i) corresponds to $g_{\Sigma\Sigma\pi} = -5.0$ and (ii) corresponds to $g_{\Sigma\Sigma\pi} = -12.0$.

Process		σ Fermilab (10^{-41} cm^2)	σ Argonne (10^{-41} cm^2)
$\nu p \to \mu^- K^+ p$		21.3	0.5
$\bar{\nu} p \to \mu^+ K^0 p$		4.6	
$\nu n \to \mu^- K^0 p$		24.7	
$\bar{\nu} n \to \mu^+ K^- n$		12.2	
$\bar{\nu} n \to \mu^+ \Lambda \pi^-$		22.6	0.62
$\bar{\nu} p \to \mu^+ \Lambda \pi^0$		24.5	
$\bar{\nu} p \to \mu^+ \Sigma^0 \pi^0$		1.9	
$\bar{\nu} p \to \mu^+ \Sigma^- \pi^+$	(i)	2.2	
	(ii)	2.6	
$\bar{\nu} n \to \mu^+ \Sigma^- \pi^0$		0.9	
$\bar{\nu} n \to \mu^+ \Sigma^0 \pi^-$		0.8	
$\bar{\nu} n \to \mu^- K^+ \Lambda$		68.3	0.35

sults clearly show that in the range of the Fermilab spectrum some of the processes have appreciable cross sections which are certainly measurable. In conclusion our results agree with the limited experimental data available. More experimental data with higher statistics is expected in the near future which can then be confronted with our theoretical results.

Note added in proof. After we had finished this work, our attention was drawn to the work of W. Macklenburg [Acta Phys. Austriaca 48, 293 (1978)], who has also considered associated production by neutrinos using a Born-term model for both charged and neutral currents.

[1]S. J. Barish *et al.*, Phys. Rev. D 19, 2521 (1978).
[2]J. Bell, *et al.*, Phys. Rev. Lett. 41, 1008 (1979); B. C. Barish, Phys. Rep. 39C, 281 (1978).
[3](a) P. Zucker and J. D. Walecka, Phys. Rev. 167, 1469 (1968); P. Zucker, J. Walecka, and P. L. Prichett, *ibid.* 184, 1825 (1969); P. A. Zucker, Phys. Rev. D 4, 3350 (1971); (b) S. Adler, Ann. Phys. (N.Y.) 50, 189 (1968); (c) G. Fogei and G. Nardulli, Nucl. Phys. B160, 116 (1979).
[4]R. E. Shrock, Phys. Rev. D 12, 2049 (1975).
[5]S. J. Barish *et al.*, Report No. ANL-HEP-PR 79-33 (unpublished); O. Erriques *et al.*, Phys. Lett. 73B, 350 (1978); W. Lerche *et al.*, *ibid.* 78B, 510 (1978); T. Bolognese *et al.*, *ibid.* 81B, 393 (1979).
[6]S. Adler, E. Paschos, and S. Nussinov, Phys. Rev. D 9, 2125 (1974).
[7]A calculation along the lines of Zucker for resonances in strange-particle channels is being considered and would be communicated later.
[8]R. Marshak, Riazuddin, and C. P. Ryan, *Theory of Weak Interactions* (Wiley Interscience, New York, 1969); S. Gasiorowicz, in *Elementary Particle Physics* (Wiley, New York, 1966).
[9]B. R. Martin, Phys. Rev. 138B, 1136 (1968); N. Zovko, Phys. Lett. 23, 143 (1966); H. Pilkhun and Jarlskog, *ibid.* 20, 428 (1966); Nature 285, 188 (1980); H. Pilkhun *et al.*, Nucl. Phys. B65, 460 (1973). For K-Λ photoproduction analysis, see F. Renard and T. Renard, Nucl. Phys. B25, 490 (1971); H. Thom, Phys. Rev. 151, 1322 (1966); T. Kuo, Phys. Rev. 129, 2264 (1963); R. L. Warnock and G. Fyre, Phys. Rev. 138B, 947 (1966).